

Grain refining of Er added to Ti–22Al–25Nb alloy and morphology of erbium precipitates

Jing-Ru Dai, Hui-Min Lu*, Zhi-Jin Cai,
Chao An

Received: 22 February 2012/Revised: 11 June 2012/Accepted: 15 June 2012/Published online: 21 February 2013
© The Nonferrous Metals Society of China and Springer-Verlag Berlin Heidelberg 2013

Abstract In order to investigate the effect of erbium (Er) on the microstructure of orthorhombic Ti_2AlNb -based alloys, four testing alloys were prepared by adding different contents of the rare earth metal Er to Ti–22Al–25Nb alloy and optical microscopy, X-ray diffraction, scanning electron microscopy, electron probe microanalysis, energy-dispersive spectrometry, and transmission electron microscopy were used. The results show that the addition of Er is capable of grain refining and the refinement effect is more obvious with increasing content of Er. The Er_2O_3 dispersoids formed by internal oxidation and Al_3Er compound particles are observed in Er-doped alloys and the number of Er precipitates is increased with increasing Er addition. It is likely that the solubility of Er in the Ti_2AlNb alloy is very low and Er precipitates tend to segregate at grain boundaries, which together with the surface activity of rare earth elements is supposed to decrease the prior B2 grain size of Ti–22Al–25Nb alloy effectively.

Keywords Ti_2AlNb -based alloys; Rare earth erbium (Er); Microstructure; Erbium precipitates

1 Introduction

In 1988, Banerjee et al. [1] identified a ternary intermetallic named O-phase (Ti_2AlNb) with orthorhombic structure for the Ti–25Al–12.5Nb composition. The ordered Ti_2AlNb -based alloys have received attractive attention as candidate materials for elevated-temperature structural applications

due to high strength-to-weight ratio, good creep properties, and excellent high-temperature performance [2–9]. Ti–22Al–25Nb alloy is one of the promising Ti_2AlNb -based alloys that have been greatly researched in recent years. Studies have shown that the mechanical properties of Ti_2AlNb -based alloys are very sensitive to the composition and microstructure, and quaternary element is added to improve microstructure and properties [6–8]. Until now, several compositions in the range of Ti–22Al–25Nb with Mo, Si, and Zr additions have been researched [10, 11] and trace elements of B, Fe, and W have been added to other Ti_2AlNb -based alloys [12–14].

Owing to unique electronic configuration, rare earths have played an important role in metallurgy and materials, such as refinement of microstructure, alloying or microalloying, and purification of materials and metamorphosis of inclusions [15], consequently resulting in properties improvement.

Recently, minor rare earth elements (REEs) have been well added to intermetallics with the purpose of microstructure modification and property improvement. To our knowledge, there are few reports about Ti_2AlNb -based alloys with Er. Up to now, studies about Y modified in Ti–17Al–27Nb, Ti–23Al–25Nb, and Ti–16Al–27Nb have been reported, respectively [16–18]. Previous research by the authors indicates that the addition of Er has a great refinement effect on the grain size and microstructure of Ti–16Al–27Nb alloy [18]. In this article, the influence of Er on the microstructure of Ti–22Al–25Nb alloy and Er precipitates was studied and discussed.

2 Experimental

The nominal compositions of the studied alloys are Ti–22Al–25Nb, Ti–22Al–25Nb–0.4Er, Ti–22Al–25Nb–0.6Er,

J.-R. Dai, H.-M. Lu*, Z.-J. Cai, C. An
School of Materials Science and Engineering, Beijing University of Aeronautics and Astronautics, Beijing 100191, China
e-mail: lhm0862002@yahoo.com.cn

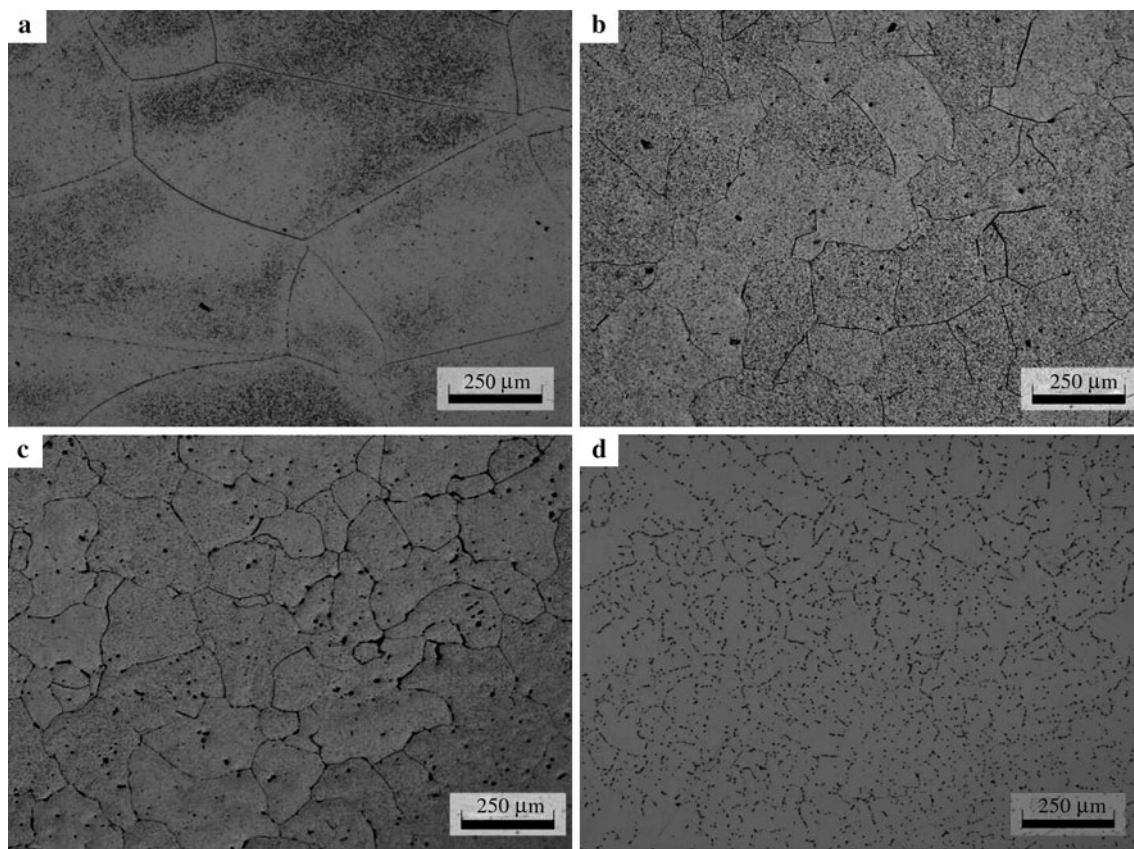


Fig. 1 Metallographic micrographs of as-cast alloys: **a** Ti-22Al-25Nb, **b** 0.4 % Er alloy, **c** 0.6 % Er alloy, and **d** 0.8 % Er alloy

and Ti-22Al-25Nb-0.8Er. All compositions are given in atomic percent. Raw materials are 99.7 % titanium sponge, 99.99 % pure aluminum, 99.88 % pure niobium, and 99.9 % pure Er.

The studied alloys were prepared in a nonconsumable electrode arc furnace with a water-cooled copper hearth in an atmosphere of argon. Each alloy button was remelted and turned over for four times to insure chemical homogeneity.

Specimen rods of 13 mm in diameter and 20 mm in length were cut using electrodischarge machine (EDM). The specimen rods were encapsulated in quartz tubing, vacuum pumped to 1.33×10^{-3} Pa, and then back-filled with argon by 2×10^4 Pa. These rods experienced solid solution processing plus aging treatment to obtain O + B2 duplex microstructure.

The microstructures and phase compositions of the alloy were conducted by optical microscopy (OM), X-ray diffraction (XRD), scanning electron microscope (SEM), electron probe microanalysis (EPMA), and transmission electron microscope equipped with an energy-dispersive spectrometer (TEM-EDS). The samples for metallographic observation were etched in Kroll reagent (HF:HNO₃:H₂O = 1:4:5). Ion beam thinning technique was used to prepare TEM samples.

3 Results and discussion

3.1 Effect of Er content on prior B2 grain size

The microstructures of the as-cast alloys are revealed in the optical micrographs presented in Fig. 1a–d. As seen in Fig. 1a, relatively coarse and nonuniform primary B2 grains are observed in nonEr alloy when no refinement measure is employed. However, the grain size is decreased gradually when increasing content of REE Er is added. Relative small grain size can be observed in 0.8 % Er alloy and there is a subtle difference in grain size as well. Besides, some black spots appear within grains or along grain boundaries that are supposed to be Er precipitates.

3.2 Phases and microstructures after heat treatment

Analysis of XRD patterns spectrum of the studied alloys after heat treatment shown in Fig. 2 reveals that all alloys comprise B2-phase and O-phase. Compared with nonEr alloy, some other XRD peaks of O-phase with different height differences are found. Furthermore, the diffraction peak of Er-rich phase is not detected by XRD with regard to

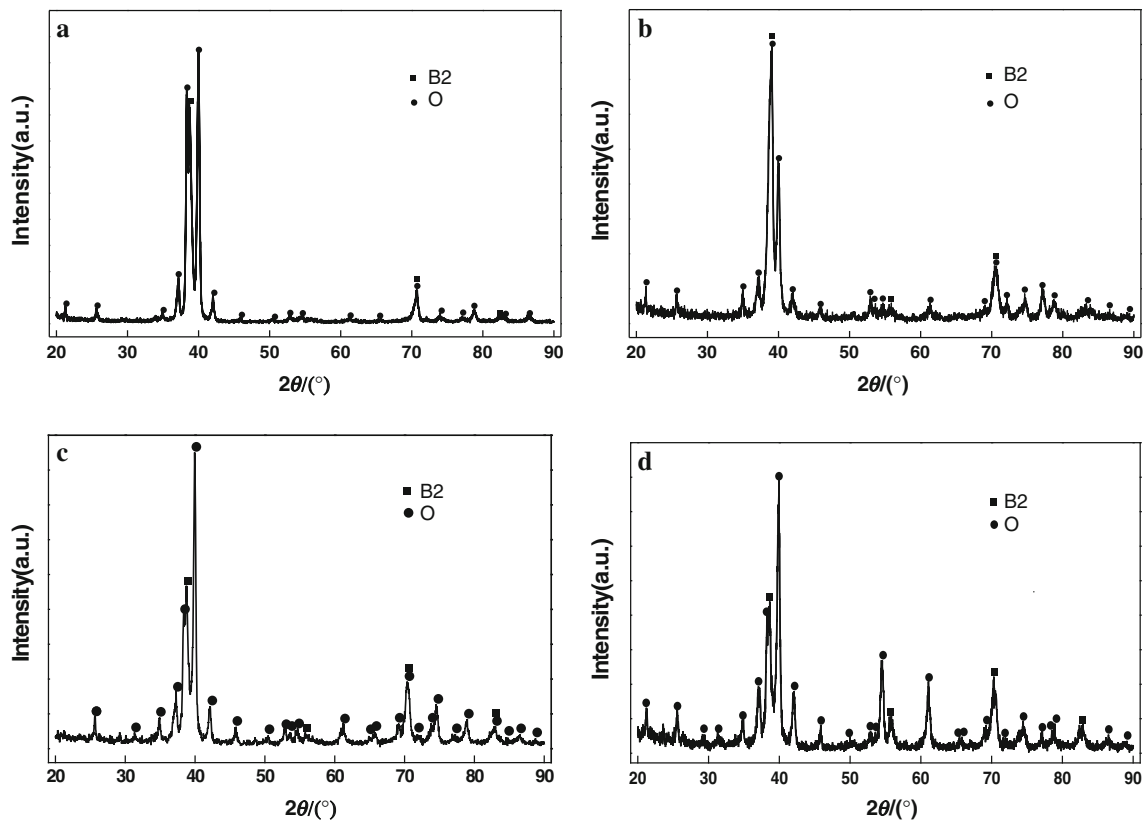


Fig. 2 XRD patterns of alloys after heat treatment: **a** Ti–22Al–25Nb, **b** 0.4 % Er alloy, **c** 0.6 % Er alloy, and **d** 0.8 % Er alloy

Er-doped alloys, which may be due to its small amount and high dispersion.

After solid solution processing plus aging treatment, microstructures of the experimental alloys are shown in Figs. 3 and 5a. The multiphase microstructures consist of lathed O-phase and equiaxed O-phase surrounded by a transformed B2 matrix in the nonEr alloy (Fig. 3), which is consistent with the detecting results of phases by XRD. However, in microstructures of Er-doped alloys, a small amount of discontinuous grain boundary phase is also observed at the prior B2 grain boundary, which is supposed to be α_2 phase based on a phase diagram [19]. Besides, Er precipitates are found both within grains and on boundaries. In these back-scattered electron images shown in Fig. 2, the light, gray, and black regions correspond to the B2, O, and α_2 phases, respectively.

As observed in Fig. 3, with increasing content of Er addition, the ratio of length to width of lathed O-phase is increased, whereas the amount of equiaxed O-phase is decreased. Certainly, specific data are needed to demonstrate the accuracy of this observation. The presence of α_2 at grain boundaries in Er-doped alloys after heat treatment reveals a compositional segregation at the grain boundaries. Furthermore, because α_2 phase is not found in nonEr alloy after the same heat treatment, it is likely that Er might

lower the transition temperature from the O + B2 binary phase area to the O + B2 + α_2 ternary phase area, which consequently leads to the presence of α_2 phase at grain boundaries as observed in the EPMA microstructures of Er-doped alloys shown in Fig. 5a.

3.3 Morphology of precipitates

From Fig. 3b–d, some white precipitates are observed both within grains and along boundaries in Er-doped alloys. As demonstrated in Fig. 3b, most precipitates are ellipsoids and clavate distributing at boundaries, whereas few large particles with irregular shape present within grains in 0.4 % Er alloy. When it refers to 0.6 % Er alloy, not only more precipitates appear but also some discontinuous net of precipitates are also observed, which leads to grain boundary segregation (Fig. 3c). In 0.8 % Er alloy, a great number of white precipitates in the shape of closed networks appear along grain boundary and grain boundary segregation becomes more severe (Fig. 3d). Through these observations, it can approximately infer that Er has a low-level solubility in Ti₂AlNb-based alloys and tends to segregate at grain boundary to lower free energy of the whole system due to the large radius difference between Er and the other elements [20]. However, exact analyses about

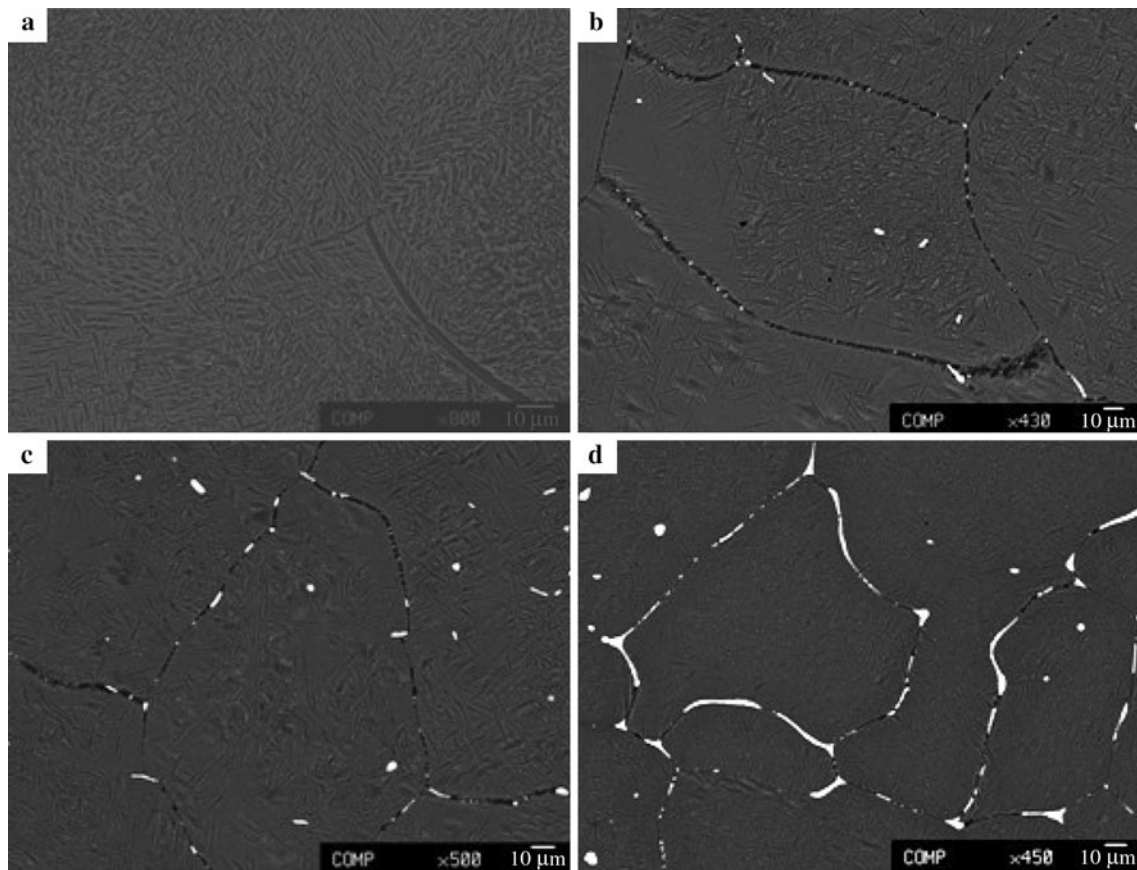


Fig. 3 BSE micrographs of alloys after heat treatment: **a** Ti-22Al-25Nb, **b** 0.4 % Er alloy, **c** 0.6 % Er alloy, and **d** 0.8 % Er alloy

Er solubility in Ti_2AlNb -based alloys are required to confirm this preliminary observation. It should also be noted that a lot of fine precipitates in white color are observed at high magnification of electron microscopy (Fig. 5a), which also are studied by TEM. Figure 4a–f indicates TEM micrographs of these studied alloys after heat treatment.

These fine particles morphology of better dispersion and ellipse are clearly observable by means of TEM scanning and observing. As seen in Fig. 4a–f, although the number of fine precipitates is increased with increasing Er addition, they share the same morphology and uniform distribution. The size of the fine precipitates can be estimated approximately at 120 nm by utilizing statistics method. It can also find that these fine precipitates tend to appear from B2-phase. To explain how these fine precipitates come out, TEM micrographs of as-cast alloys are presented in Fig. 4g, h. It seems reasonable that these fine precipitates are formed during aging process for no fine particles in nanometer-scale are found in the as-cast alloys.

3.4 Components analysis of precipitates

The SEM micrographs of Ti-22Al-25Nb-0.6Er alloy after heat treatment showing both submicron precipitates and

nanometer particles with white color (Fig. 5a, b) illustrate that they both contain heavy REE Er. SEM-EDS and TEM-EDS were used to analyze the phase components of both submicron precipitates and nanometer-scale precipitates, respectively, with the corresponding experimental results shown in Table 1. Also, the EDX analysis results of precipitates in 0.6 % Er alloy shown in Table 1 corresponded to A, B, and C spots in Fig. 5. According to the EDX spectrum analysis (Table 1), some precipitates are Er-rich oxides, consisting most of the Er and O. Because the stoichiometric ratio between Er and O is approximately 2:3, the chemical formula is supposed to be Er_2O_3 . In addition, it seems that the probability that Er_2O_3 appears in 0.4 % Er alloy is higher than both 0.6 % Er alloy and 0.8 % Er alloy. Thus, it can be inferred that the formation of Er_2O_3 has occurred first. Figure 5 shows the results of line scan of electronic probe of Ti-22Al-25Nb-0.6Er alloy. It indicates that these big granular precipitates are composed of two elements: Al and Er. It is reasonable that a compound of Al and Er is preferred to form among the Ti-Al-Nb-Er system because the electronegative difference between Al and Er is the largest. The electronegative values of Ti, Al, Nb, and Er are 1.54, 1.61, 1.6, and 1.24, respectively. It could also be concluded that Er mainly

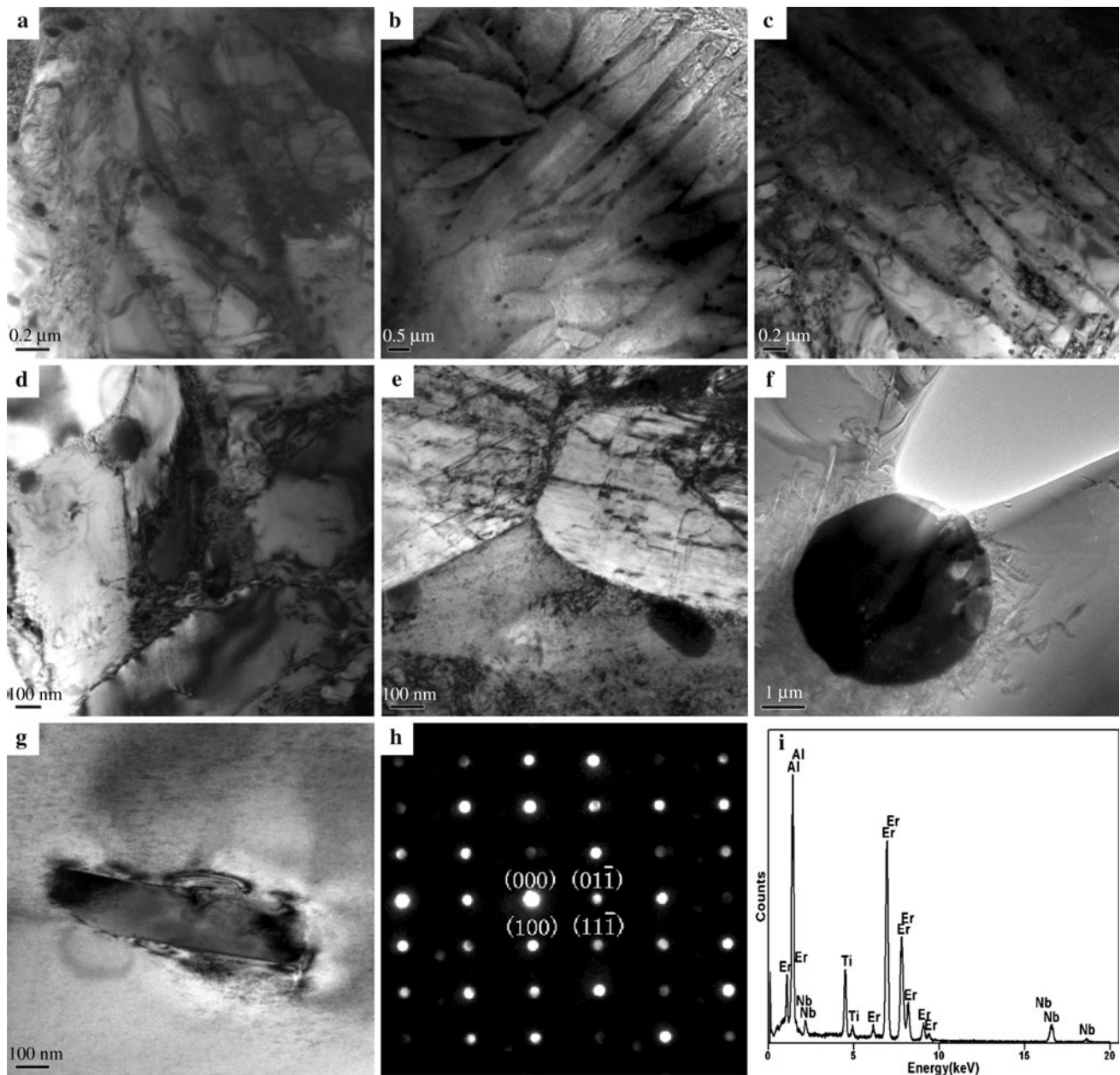


Fig. 4 TEM micrographs of alloy and analysis of fine precipitates. **a** precipitates in 0.4 % Er alloy, **b** precipitates in 0.6 % Er alloy, **c** precipitates in 0.8 % Er alloy, **d** and **e** pinning effect of erbium precipitate on triple boundary junctions in 0.4 % and 0.6 % Er alloys,

respectively, **f** and **g** images of as-cast alloys, **h** selected area electron diffraction (SAED) of fine precipitates, and **i** EDS analysis of fine precipitated phase in (a)–(c)

exists in the white precipitated phase for the big atomic number of Er. TEM–EDS results confirmed that those nanometer-scale precipitates have been mainly consisted of Al and Er, with the similar composition with biggish precipitates. Combined with the Al–Er binary alloy phase diagram [21] and the SAED results that the crystal structure of fine precipitated phase is simple cubic with a lattice parameter of 0.4215 nm, it can be concluded that the precipitated phase is Al_3Er phase, which may have precipitated from the matrix during aging treatment compared

with the TEM microstructures of the as-cast alloys before heat treatment. It is assumed that the formation of these fine Er particles might bring improvement in mechanical property, which will be further investigated.

3.5 Mechanism of grain refinement

The REEs, due to their surface activity, are able to lower the surface tension of liquid metal and thus decrease the fluctuated energy needed for the formation of critical grain

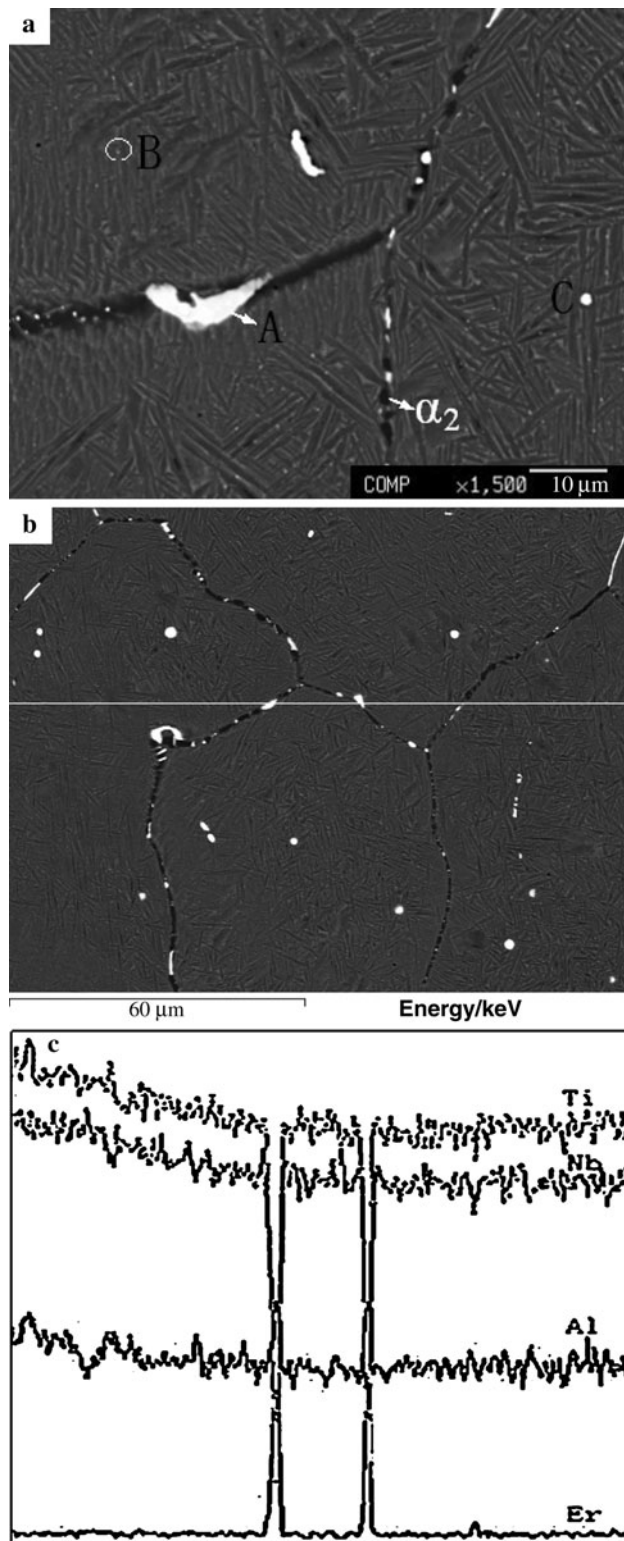


Fig. 5 EPMA images of 0.6 % Er alloy after heat treatment: **a** discontinuous α_2 phase at grain boundaries, appearances, and distributions of erbium-rich phases, **b** microstructure, and **c** line distribution of elements corresponding to **b**

Table 1 Results of composition analysis of erbium particles appearing in micrographs of experimental alloys (at%)

Alloys	O	Al	Ti	Nb	Er
0.4 % Er alloy	52.64	7.70	3.97	2.67	33.02
0.4 % Er alloy	–	44.51	18.54	3.88	33.06
0.4 % Er alloy	–	67.97	8.37	6.01	17.64
0.6 % Er alloy (A)	58.21	0.00	7.57	5.66	28.55
0.6 % Er alloy (B)	–	32.98	19.45	13.85	33.70
0.6 % Er alloy (C)	–	47.95	17.15	4.74	30.16
0.8 % Er alloy	59.82	0.00	3.09	1.29	35.79
0.8 % Er alloy	–	48.83	17.04	4.25	29.87
0.8 % Er alloy	–	40.06	12.68	9.28	37.96

nuclei. Consequently, both the probability and the growth rate of nucleation are enhanced.

The particles of Al_3Er preferentially precipitated in the process of crystallization, together with impurities O acting as nucleating sites, also contribute to grain refinement.

The existence of nanometer-scale Al_3Er precipitates in Ti–Al–Nb–Er system after heat treatment proves that a small part of Er has once solubilized in the matrix and then decomposed from the matrix. However, most Er with a high-segregation tendency segregates at boundaries during the cooling process and consequently leads to the formation of Al_3Er . The primary Al_3Er precipitates, acting as heterogeneous nucleation site, play an important role in refining grain size. They also function as obstacles to the migration of boundaries. In addition, with increasing content of Er, the shape of Al_3Er phase would transfer from discontinuously distribution to continuously distribution, which effectively prevented grain from growing.

It can be concluded that it is the heterogeneous nucleation function and obstruction effect of Al_3Er on grain boundary migration that mainly contribute to the grain refinement in the experimental alloy.

4 Conclusion

Addition of Er to Ti_2AlNb -based alloys contributes to grain refinement and the refinement effect is gradually obvious with increasing content of Er.

It is likely that Er may lower the transition temperature from the O + B2 binary phase area to O + B2 + α_2 ternary phase area, as a small amount of discontinuous α_2 is observed at the B2 boundary only in Er-doped alloys after heat treatment.

Erbium (Er) has a low-level solubility in Ti_2AlNb -based alloys and has a high-segregation tendency at grain boundaries.

An Er-rich phase named Al_3Er is formed. Primary Al_3Er particles formed during solidification, which act as heterogeneous nucleus and also are capable of impeding boundary movement, play an important role in grain refinement. In addition, Er_2O_3 is also formed by internal oxidation.

Acknowledgments This study was financially supported by the Science and Technology Ministry of China to the National High Technology “863” Project (No. 2012AA062302).

References

- [1] Banerjee D, Gogia AK, Nandy TK, Joshi VA. A new ordered orthorhombic phase in a Ti_3Al alloy. *Acta Metall.* 1988;36(4):871.
- [2] Chu F, Mitchell TE, Manjumdar B, Mriacle D, Nandy TK, Banerjee D. Elastic properties of O phase in Ti–Al–Nb alloys. *Intermetallics.* 1997;5(2):147.
- [3] Gogia AK, Nandy TK, Banerjee D, Carisey T, Strudel JL, Franchet JM. Microstructure and mechanical properties of orthorhombic alloy in the Ti–Al–Nb system. *Intermetallics.* 1998;6(7–8):741–8.
- [4] Nandy TK, Banerjee D. Creep of the orthorhombic phase based on the intermetallic Ti_2AlNb . *Intermetallics.* 2000;8(5–6):915–28.
- [5] Mao Y, Li SQ, Zhang JW, Peng JH, Zou DX, Zhong ZY. Microstructure and tensile properties of orthorhombic Ti–Al–Nb alloys. *Intermetallics.* 2000;8(5–6):659–62.
- [6] Shagiev MR, Galejev RM, Valiakhmetov OR, Safiullin RV. Improved mechanical properties of Ti_2AlNb -based intermetallic alloys and composites. *Adv Mater.* 2009;59(13):105–8.
- [7] Muraleedharan K, Nandy TK, Banerjee D, Lele S. Phase stability and ordering behaviour of the O phase in Ti–Al–Nb alloys. *Intermetallics.* 1995;3(3):187.
- [8] Tang F, Nakazawa S, Hagiwara M. The effect of quaternary additions on the microstructures and mechanical properties of orthorhombic Ti_2AlNb -based alloys. *Mater Sci Eng A.* 2002;329–331:492–8.
- [9] Germann L, Danerjee D, Guedou JY, Strudel JL. Effect of composition on the mechanical properties of newly developed Ti_2AlNb -based titanium aluminide. *Intermetallics.* 2005;13(9):920–4.
- [10] Carisey TE, Gogia AK, Strudel J, Banerjee D. Titanium-based intermetallic alloys of the Ti_2AlNb type with high yield strength and good creep resistance. European Patent, no. 0924308. 2002.
- [11] Carisey TE, Banerjee D, Franchet JM, Gogia AK. Titanium-based intermetallic alloys. US Patent, no. 6, 132, 526. 2000.
- [12] Yang SJ, Nam SW, Hagowara M. Phase identification and effect of W on the microstructure and micro-hardness of Ti_2AlNb -based intermetallic alloys. *J Alloy Compd.* 2003;350(1–2):280–7.
- [13] Satoshi E, Kaneaki T, Koichi T. Improvement of room temperature ductility for Mo and Fe modified Ti_2AlNb alloy. *Mater Sci Eng A.* 2010;528(1):355–62.
- [14] Tang F, Shizuo N, Hagowara M. Effect of boron microalloying on microstructure, tensile properties and creep behavior of Ti–22Al–20Nb–2W alloy. *Mater Sci Eng A.* 2001;315(1–2):147–52.
- [15] Li DQ, Wang QD, Ding WJ. Effects of Ho on the microstructure and mechanical properties of Mg–Zn–Ho–Zr magnesium alloys. *Rare Met.* 2011;30(2):131.
- [16] Chen YY, Si YF, Kong FT, Liu ZG, Li JW. Effects of yttrium on microstructures and properties of Ti–17Al–27Nb alloy. *Trans Nonferrous Met Soc China.* 2006;16(2):316–20.
- [17] Si YF, Cheng YY, Liu ZG, Kong FT. Influence of yttrium on microstructure and properties of Ti–23Al–25Nb alloy after heat treatment. *Trans Nonferrous Met Soc China.* 2006;16(Suppl 2):849–53.
- [18] Ke YB, Duan HP, Sun YR. Effect of yttrium and erbium on the microstructure and mechanical properties of Ti–Al–Nb alloys. *Mater Sci Eng A.* 2010;528(1):220–5.
- [19] Su MK, Zheng LJ, Lang B, Yan J, Zhang H. Microstructural evolution of a PM TiAl alloy during heat treatment in $\alpha+\gamma$ phase field. *Rare Met.* 2012;31(5):424.
- [20] Zhang YG, Hang YF, Chen G. High temperature intermetallic alloys. Beijing: National Defense Industry Press; 2001. p. 789–97.
- [21] Zhang FZ, Gu LJ. Al-REE binary phase diagram. Beijing: China Academic Journal Electronic Publishing House; 1994–2010. p. 65.